ELSEVIER

Atmospheric Research 72 (2004) 365–382

ATMOSPHERIC RESEARCH

www.elsevier.com/locate/atmos

Performance of Goddard earth observing system GCM column radiation models under heterogeneous cloud conditions

L. Oreopoulos[a,b,*], M.-D. Chou[b,1], M. Khairoutdinov[c], H.W. Barker[d], R.F. Cahalan[b]

[a] *JCET-University of Maryland Baltimore County, Baltimore, MD, USA*
[b] *Laboratory for Atmospheres, NASA Goddard Space Flight Center, Code 913, Greenbelt, MD 20771, USA*
[c] *Dept. of Atmospheric Sciences, Colorado State University, Fort Collins, CO, USA*
[d] *Meteorological Service of Canada, Downsview, ON, Canada*

Received 30 July 2003; received in revised form 19 December 2003; accepted 31 March 2004

Abstract

We test the performance of the shortwave (SW) and longwave (LW) Column Radiation Models (CORAMs) of Chou and collaborators with heterogeneous cloud fields from a single-day global dataset produced by NCAR's Community Atmospheric Model (CAM) with a 2-D Cloud Resolving Model (CRM) installed in each column. The original SW version of the CORAM performs quite well compared to reference Independent Column Approximation (ICA) calculations for boundary fluxes (global error ~ 4 W m^{-2} for reflected flux), largely due to the success of a combined overlap and cloud scaling parameterization scheme. The absolute magnitude of errors relative to ICA are even smaller (global error ~ 2 W m^{-2} for outgoing flux) for the LW CORAM which applies similar overlap. The vertical distribution of heating and cooling within the atmosphere is also simulated quite well with daily averaged zonal errors always less than 0.3 K/day for SW and 0.6 K/day for LW heating (cooling) rates. The SW CORAM's performance improves by introducing a scheme that accounts for cloud inhomogeneity based on the Gamma Weighted Two Stream Approximation (GWTSA).

These results suggest that previous studies demonstrating the inaccuracy of plane-parallel models may have unfairly focused on worst case scenarios, and that current radiative transfer algorithms in General Circulation Models (GCMs) may be more capable than previously thought in estimating realistic spatial and temporal averages of radiative fluxes, as long as they are provided with correct mean cloud profiles. However, even if the errors of our particular CORAMs are small,

* Corresponding author. Laboratory for Atmospheres, NASA Goddard Space Flight Center, Code 913, Greenbelt, MD 20815, USA. Tel.: +1-301-614-6128; fax: +1-301-614-6307.
E-mail address: lazaros@climate.gsfc.nasa.gov (L. Oreopoulos).
[1] Current address: Dept. of Atmospheric Sciences, National Taiwan University, Taipei, Taiwan.

0169-8095/$ - see front matter © 2004 Elsevier B.V. All rights reserved.
doi:10.1016/j.atmosres.2004.03.025

they seem to be systematic, and their impact can be fully assessed only with GCM climate simulations.
© 2004 Elsevier B.V. All rights reserved.

Keywords: Goddard earth observing system; General Circulation Model; Column radiation model

1. Introduction

Numerous efforts have been expended during the past few years to quantify the effects of cloud water horizontal inhomogeneity on the radiative properties of clouds. Most of these efforts have concentrated on solar wavelengths rather than in infrared wavelengths where cloud emissivity saturates at relatively low values of cloud optical depth, and errors are generally smaller. In a recent paper, Rossow et al. (2002) surveyed the literature for observational studies of the shortwave (SW) impact of neglecting cloud horizontal inhomogeneity and found a wide range of 0.025 to 0.3 for albedo bias estimates. This range of estimates, however, did not correspond to global averages, but values estimated under a variety of conditions and for different cloud types.

Given the potentially large SW radiative impact of horizontal cloud heterogeneities, it was only logical that research efforts would be directed towards developing algorithms that account for them in modeling applications while being as simple as possible, ideally following plane-parallel formalisms. Clearly, the algorithms developed with single-layer cloud systems in mind (Cahalan et al., 1994; Barker, 1996; Cairns et al., 2000; Szczap et al., 2000a,b) are not strictly suitable for General Circulation Models (GCMs), which use multi-layer algorithms that are not necessarily straightforward extensions of their single-layer counterparts. The first complete inhomogeneous solar algorithm conforming to GCM requirements was developed by Oreopoulos and Barker (1999). Modifications and improvements on the basic concept of this algorithm in terms of computational speed and concurrent treatment of vertical cloud variability followed in publications by Barker and Fu (2000) and Kato (2003). Around the same time, algorithms that take into account the inhomogeneous nature of clouds at the longwave (LW) part of the spectrum were also developed (Li and Barker, 2002).

The main purpose of this paper is to present an evaluation of the performance under inhomogeneous cloud conditions of two Column Radiation Models (CORAMs) developed by Chou and collaborators (see references), and used in various NASA-Goddard GCMs. Since, however, the cloud statistics needed for input are derived from the same cloud distributions used in our reference (“truth”) calculations, the errors presented in the following are not in any way typical of the radiation budget errors that would arise in GCM simulations using these CORAMs. Instead, they are typical errors that would arise if perfect cloud statistics, suited to the input needs of the specific CORAMs, were used. Extended tests with more sophisticated research versions of the CORAM that account for cloud inhomogeneity is not a top priority in this study, but some relevant findings will be shown for the SW CORAM (which grabs the lion’s share of our analysis). The CORAMs are evaluated on global scales, but with the caveat that the input cloud data come from only one simulated day. Still, this is an improvement over previous studies where

assessments of the errors of plane-parallel homogeneous (PPH) codes were made with a limited number of cloud fields generated either by theoretical fractal models (e.g. Cahalan et al., 1994), or by Cloud Resolving Models (CRMs) attempting to simulate clouds of only one particular type (e.g. Barker et al., 1999; Barker and Fu, 1999), or clouds of a specific field campaign (Fu et al., 2000).

The present paper has been organized as follows: We present a description of the input data set in Section 2, a description of the CORAMs in Section 3, and results from the SW and LW experiments in Sections 4 and 5, respectively. We close with a discussion on our findings in Section 6.

2. Dataset: CAM/CRM clouds

Recently, Khairoutdinov et al. (in press) embedded a 2-D version of the 3-D CRM described in detail by Khairoutdinov and Randall (2003) into each grid column of NCAR's Community Atmosphere Model (CAM, the atmospheric component of the Community Climate System Model GCM) version 1.8, to serve as a super-parameterization of clouds (for an earlier implementation of this idea see Khairoutdinov and Randall, 2001). We have selected a single day (January 1) from a 500-day-long simulation with the super-parameterization, initialized on September 1st, and using T42 resolution ($2.8 \times 2.8^\circ$ grid) with 26 vertical layers (24 for the CRM itself, at the same levels as the lowest 24 layers of the CAM). The cloud fields used as input in our radiative transfer calculations with the CORAMs come from 24 global "snapshots" saved at 1-h intervals for this day. The same snapshots were also used in a recent study by Räisänen et al. (in press). Within each of the 64×128 gridboxes covering the globe, clouds are then resolved in 64 columns of 4 km horizontal width aligned in the west–east direction, and 24 vertical layers.

Fig. 1 shows latitude–height (zonally averaged) cross-sections of daily averaged (i.e. averaged over the 24 snapshots) cloud properties for each model layer: cloud fraction, total water path (liquid water path + ice water path), and cloud inhomogeneity parameter ν of Barker (1996) calculated from the method of moments (MOM) as the square of the ratio of mean to standard deviation of the water path in each layer. These figures show that the super-parameterization within the CAM captures the main contrast in cloud types between tropics and mid-latitudes: clouds in the tropics are higher in the troposphere, thicker, and more heterogeneous (smaller values of ν). Khairoutdinov et al. (in press) further discuss the degree of realism of various output fields from the entire experiment.

3. The column radiation models

We use both the SW and LW CORAMs developed by M.-D. Chou and collaborators and implemented in various NASA-GSFC GCMs. These CORAMs are described in Chou et al. (1998, 2001) and Chou and Suarez (1999).

Some of the most recent changes in the SW CORAM are the inclusion of variable cloud particle size (r_e) that depends on water content, following McFarquhar (2001) for ice clouds, and Szczodrak et al. (2001) for liquid clouds, and of a new parameterization for ice

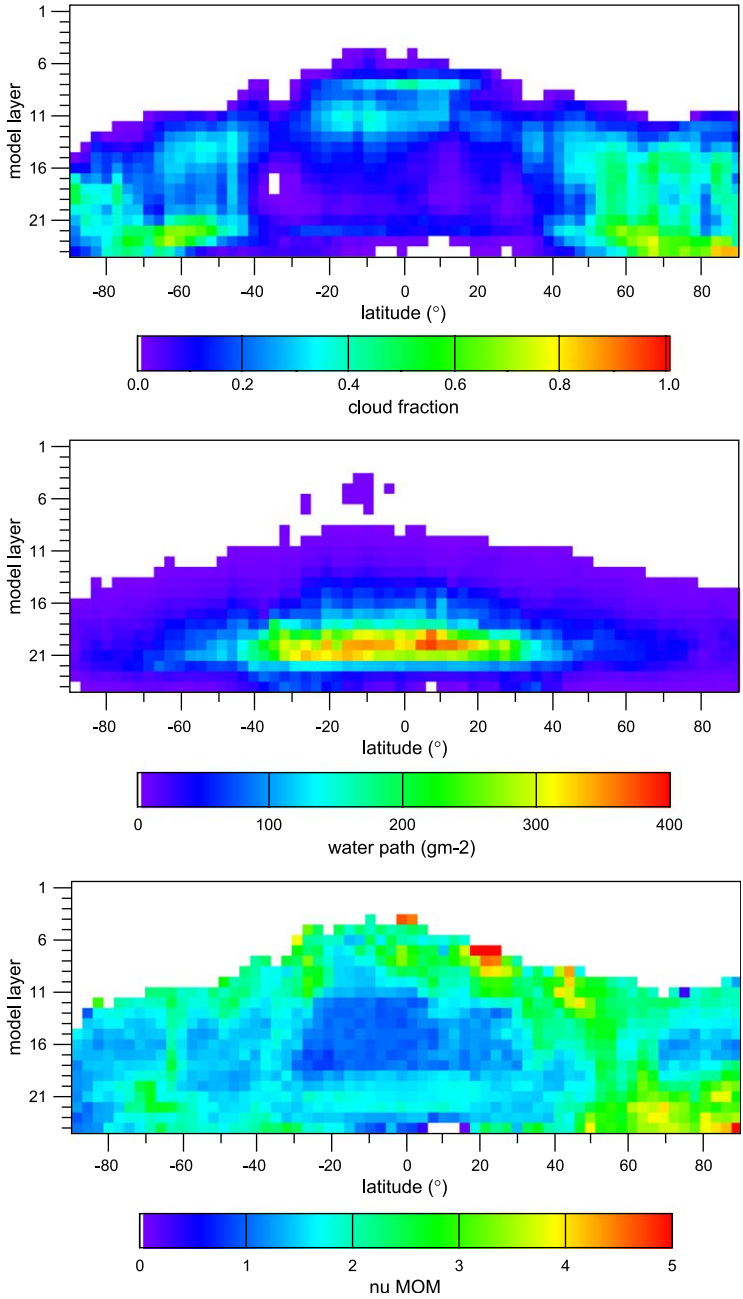

Fig. 1. Daily averaged zonal profiles of layer cloud fraction, water path, and inhomogeneity parameter *v*. Layer indices are assigned from the top down.

particle single-scattering albedo (Chou et al., 2002). We will discuss the implications of the first of these changes in our calculations in the following section. An important feature of the SW CORAM is the cloud overlap treatment which is schematically shown in Fig. 2. Clouds are grouped into three categories: low, middle and high, separated at 700 and 400 hPa. Through two separate optical depth adjustments ($\tau \rightarrow \tau_{dd}$, $\tau \rightarrow \tau_{df}$).

$$\tau_{dd} = \chi_{dd}\tau \tag{1a}$$

$$\tau_{df} = \chi_{df}\tau \tag{1b}$$

which preserve the layer albedo (R_{dd}, R_{df}) for direct (dd) and diffuse (df) incident radiation

$$R_{dd}(\tau_{dd},\ r_e, \mu_0) = q\ R_{dd}(\tau,\ r_e,\ \mu_0) \tag{1c}$$

$$R_{df}(\tau_{df},\ r_e) = q\ R_{df}(\tau,\ r_e) \tag{1d}$$

$$q = C_i/C_{j,\max} \tag{1e}$$

the cloud in any layer i that has smaller cloud fraction (C_i) than the maximum cloud fraction within its group j ($C_{j,\max}$), is "stretched" and "thinned" so that it acquires this maximum value (for details see Chou et al., 1998). The adjustment parameters χ_{dd} and χ_{df} are functions of q, τ, and (in the case of χ_{dd}) the cosine of the solar zenith angle (SZA), μ_0. Once this adjustment is made, each cloud group is characterized by its own unique cloud fraction $C_{j,\max}$. Clouds among different groups are assumed to overlap randomly. Clearly, the concept is inspired from the observations of Tian and Curry (1989) that neighboring clouds tend to overlap maximally, while clouds separated by clear skies tend to overlap randomly. This overlap assumption allows each gridbox to be divided into $\leq 2^j$ sub-columns ($j \leq 3$) where each layer is either completely cloudy or cloud-free (Fig. 2, right), and for which the full vertical distribution of fluxes can be easily calculated. The weighted average of the sub-column estimates gives the mean for the entire gridbox, and can be thought of as a "crude" Independent Column Approximation (ICA).

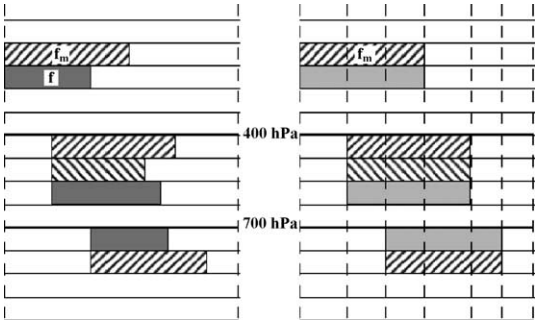

Fig. 2. Sketch of how cloud overlap (left) and optical thickness scaling (right) is implemented in the SW CORAM (adapted from Chou and Suarez, 1999).

For LW calculations, the concept of the probability of clear line-of-sight of Harshvardhan et al. (1987) is used to calculate the flux transmittance between two different layers. Clouds are again grouped into three different height ranges, as in Fig. 2, with maximum overlap assumed within each group, and random overlap between groups. Probabilities of clear line-of-sight are calculated for each group, and the total probability between any two levels is the product of probabilities of the cloud groups contained within these levels. For details the reader is referred to Chou et al. (2001, p. 31–34).

4. SW experiments

For our broadband SW calculations we performed four different sets of runs: two sets with the original version of the CORAM and two with modified versions. Each set consisted of runs for each gridbox receiving non-zero solar illumination calculated according to its center latitude and longitude coordinates and according to the Greenwich Mean Time (GMT) corresponding to the particular snapshot. The original version of the CORAM was used for ICA and PPH runs. The ICA runs were performed as follows: the CORAM was run for each of the 64 CRM sub-columns of the gridbox with the cloud fraction of each layer of a sub-column either 0 or 1, and with a particle size profile that depended on the water content profile according to McFarquhar (2001) and Szczodrak (2001); the gridbox-mean (ICA) fluxes were derived by averaging the results for the 64 sub-columns. Note that the discussion pertaining to Fig. 2 becomes irrelevant for ICA runs because of the binary nature of layer cloud fraction. The PPH runs were performed as follows: for each vertical layer, the cloud fraction, and the mean liquid and ice water paths were determined for the gridbox; the particle sizes of each phase were estimated from the individual mean water paths; the CORAM in its original form was applied to each gridbox using as input these cloud fraction, water path and particle size profiles.

One of the modified versions of the CORAM, called "PPH random", was designed to reveal the impact of the cloud adjustment and overlap parameterizations depicted in Fig. 2. In this PPH variant, the albedo and transmittance of a layer i was calculated as the weighted average of the corresponding clear and cloudy fractional fluxes:

$$f_i = (1 - C_i) f_{\mathrm{clr},i} + C_i f_{\mathrm{cld},i} \tag{2}$$

where f_i, $f_{\mathrm{clr},i}$, $f_{\mathrm{cld},i}$ are one of albedo, diffuse transmittance and direct transmittance of the entire layer i and of the clear and cloudy parts, respectively. The flux profile was then determined by radiatively linking the f_i's (see Eqs. (6.9)–(6.16) in Chou and Suarez, 1999). As explained in Oreopoulos and Barker (1999) and Barker et al. (1999), because this type of linking does not preserve any information on whether the flux transmitted and reflected to a layer comes from the clear or cloudy parts of the layers above and below, it is for all practical purposes equivalent to an indiscriminate application of the random overlap assumption for all layers, regardless of whether they are contiguous or not.

The other modified version is based on the Gamma Weighted Two Stream Approximation (GWTSA) of Oreopoulos and Barker (1999) where the direct beam and δ-Eddington PPH solutions $f_{\mathrm{PPH},i}$ of layer i are replaced by their counterpart analytic

solutions $f_{\Gamma,i}$ obtained by integrating over a gamma distribution of optical depths $p_\Gamma(\tau)$ with mean optical depth $\bar{\tau}$ and variability (shape) parameter $\nu=(\bar{\tau}/\sigma)^2$ (σ is the standard deviation of the optical depth distribution):

$$f_{\Gamma,i} = \int_0^\infty p_\Gamma(\tau) f_{\mathrm{PPH},i} \mathrm{d}\tau \tag{3a}$$

$$p_\Gamma(\tau) = \frac{1}{\Gamma(\nu)} \left(\frac{\nu}{\bar{\tau}}\right)^\nu \tau^{\nu-1} \mathrm{e}^{-\nu\tau/\bar{\tau}} \tag{3b}$$

$\Gamma(\nu)$ is the gamma function. The solutions of Eq. (3a) for reflectance, diffuse transmittance and direct transmittance can be found in Appendix A of Oreopoulos and Barker (1999). Whenever skies are clear, the original δ-Eddington PPH solutions of the CORAM are invoked for direct incidence. For diffuse incidence on clear skies, the PPH solutions of Meador and Weaver (1980) are implemented, replacing the previously used empirical approximation of setting the SZA to 53° in the solutions for direct incidence (Chou and Suarez, 1999).

The actual implementation in the Goddard SW CORAM differs from the one described by Oreopoulos and Barker (1999) in several ways: first, the scaling of optical depth conveyed by Eqs. (1a)–(1e) is retained; second the cloud optical depth adjustment described in their paper by Eqs. (21–22) is omitted; third, MOM estimates of ν are used instead of maximum likelihood estimates; and fourth, ν is estimated from the water path variability. The latter value of ν is not identical to the value derived from the optical depth variability, as was the case in Oreopoulos and Barker (1999) who used a constant particle size assumption. Estimating ν from the water path variability is a simplifying approximation, since the spectral dependence of optical depth does not translate to spectral dependence of ν. It is also consistent with potential future implementations of GWTSA in GCMs which are more likely to be able to only predict subgrid water path variability, and not subgrid variable of particle size (unless a constant droplet number density assumption is invoked). Attempting to remain more faithful to the original implementation of Oreopoulos and Barker (1999) would force us to abandon essential features of the Chou et al. SW CORAM, while not necessarily providing better performance (according to test calculations).

All the results that follow are averaged over the 24 snapshots (daily averages), and the rms errors relative to the ICA are calculated using these daily averages, i.e. the rms errors encompass only spatial and not temporal differences. As mentioned before, our runs used a realistic global distribution of SZAs for each of the snapshots of January 1, so we can express the SW CORAM performance results in energy units W m^{-2}. The SW surface albedo was assumed to be spectrally independent and invariable to SZA variations or the presence of clouds (which largely regulate the relative amounts of direct and diffuse solar irradiance reaching the ground). We used the broadband albedo values from a February 1–5 simulation of the Meteo France ARPEGE GCM (Räisänen, 1999). Aerosols were neglected, and the ozone profile of a standard midlatitude summer atmosphere was used for all gridboxes. ICA is our reference (“truth”) estimate. Barker et al. (1999) and others

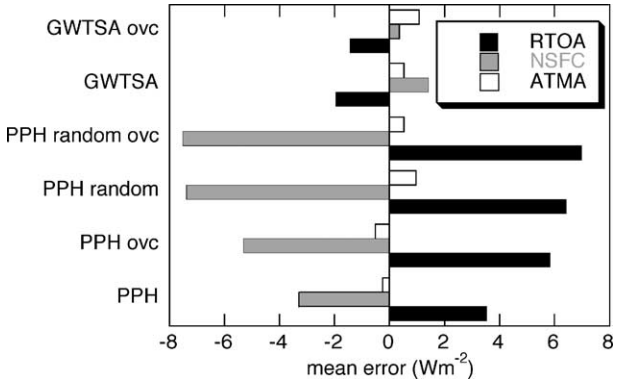

Fig. 3. Daily averaged global SW flux errors for all or just overcast ("ovc") gridboxes.

have shown that domain and daily averaged errors of ICA are small relative to full 3D Monte Carlo calculations for most cloud fields.

Fig. 3 shows the global mean errors relative to the ICA for the three different versions of the SW CORAM and for the following quantities: reflected flux at the top-of-the-atmosphere (RTOA), net flux absorbed at the surface (NSFC), and net flux absorbed within the atmosphere (ATMA). Averages are shown for all gridboxes as well as gridboxes that are overcast on a daily averaged basis (~ 1500 gridboxes, "ovc"). Errors in RTOA and NSFC are of opposite sign (positive sign indicates overestimate relative to ICA), as expected, and of about equal magnitude. Consequently, mean errors in ATMA are very small. PPH overestimates global RTOA by ~ 4 W m^{-2}, PPH random increases the error more than 50% (~ 100% for NSFC), and GWTSA reduces it by about the same amount, while changing the sign of the error. Interestingly, when only overcast gridboxes are considered, the GWTSA performance improves for RTOA and NSFC, in contrast to PPH

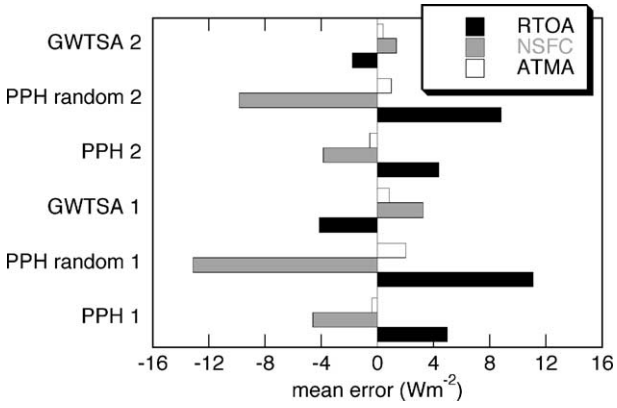

Fig. 4. Daily averaged global SW flux errors for gridboxes with mean (cloudy sub-columns only) atmospheric column-integrated water path greater 200 g m^{-2} ("1") and gridboxes with v of column-integrated water path less than 1.5 ("2").

and PPH random for which it deteriorates. Overall, however, the errors are far smaller than previously reported in studies of individual cloud systems (Barker et al., 1999; Oreopoulos and Barker, 1999; Barker and Fu, 1999).

The PPH error increases only modestly when gridboxes with either thick or strongly inhomogeneous clouds are averaged separately. This is shown in Fig. 4 which summarizes global average (also properly area-weighted) errors for gridboxes with mean (over cloudy sub-columns only) column-integrated water path (daily averaged) greater than 200 g m^{-2} ($\sim$ 2100 gridboxes) and gridboxes with v of column-integrated water path less than 1.5 ($\sim$ 2600 gridboxes). The difference between PPH and PPH random is, however, much larger than in Fig. 3. GWTSA reduces the errors significantly for the subset of gridboxes with $v < 1.5$, but has a smaller impact for the subset with large water paths.

The next point of interest would naturally be the geographical distribution of errors. The latitudinal behavior is highlighted in Fig. 5 which shows the zonally averaged mean and rms errors for RTOA. As before, prior daily averaging has been performed, and

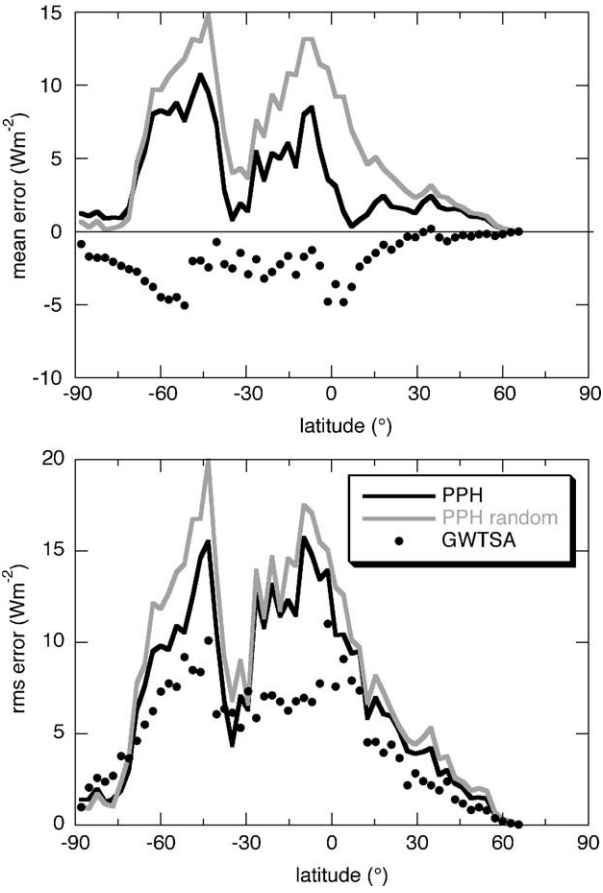

Fig. 5. Daily averaged zonal SW flux mean errors for RTOA (top) and corresponding rms errors (bottom).

negative mean error values indicate underestimates relative to the ICA. It is immediately apparent that the latitudinal variation of PPH and PPH random errors is consistent with the cloud properties shown in Fig. 1. Thick and inhomogeneous clouds just south of the equator result in PPH errors approaching 10 W m^{-2}, which GWTSA reduces by a factor of almost 5. Around 5°N, the PPH error has a local minimum, and the GWTSA a local maximum, but for the PPH this is largely a result of error cancellation as the bottom panel (rms errors) reveals. Since errors are expressed in flux units of W m^{-2}, the amount of available solar insolation is a major factor in determining their magnitude. Thus, we see much greater errors in the mid-latitudes of the southern hemisphere (SH) than the mid-latitudes of the northern hemisphere (NH), despite the fact that the cloud water path and inhomogeneity are only moderately higher in the SH.

Some interesting conclusions can also be drawn by studying the distribution of errors for individual gridboxes (no geographic averaging). Fig. 6, for example, shows the daily averaged RTOA errors of all gridboxes by plotting PPH random and GWTSA errors vs. PPH errors. We see that PPH errors can occasionally become negative (PPH underestimates TOA reflected flux) which seems to conflict with the well-ingrained perception that PPH always overestimates the albedo of inhomogeneous cloudy atmospheres. The reason that PPH underestimates occur in our results is that we are dealing with a multi-layer atmosphere with many layers partially filled with clouds so that the scalings of Eqs. (1a)–(1e) are often invoked. The final cloud fraction and optical depth profile that is used as input into the PPH run can occasionally result in smaller reflected and larger transmitted fluxes than the ICA run for which the exact optical depth and relative vertical location of clouds is known. When the PPH underestimates, it performs always better than the

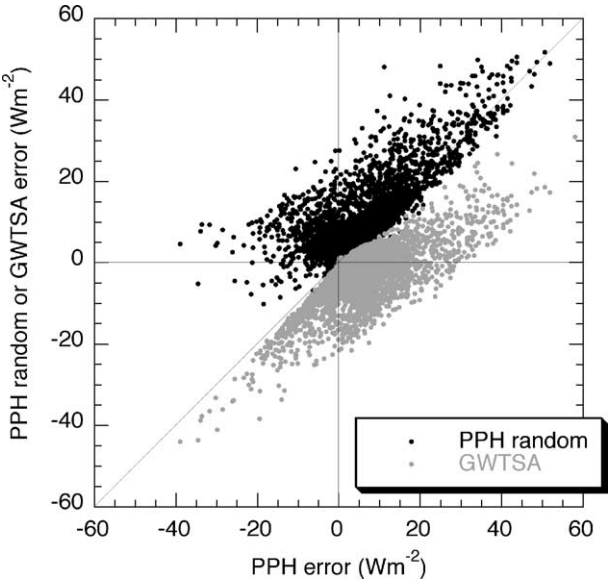

Fig. 6. RTOA PPH random and GWTSA errors vs. PPH errors for the entire portion of the globe receiving solar illumination. Each point is the daily average of one gridbox.

GWTSA (points below the diagonal in the lower left quadrant). The reason is that the current version of the CORAM with GWTSA keeps the scalings of the original PPH version, while also reducing the albedo of each cloudy layer by replacing the two-stream PPH solutions with their counterpart GWTSA solutions. On the other hand, PPH random version changes the values of the flux profile so drastically that the sign of the error reverses (upper two quadrants). Indeed, it is extremely rare that PPH random will underestimate the reflectance since the indiscriminate application of random overlap almost always overestimates cloud fraction, and thus maximizes the amount of clouds exposed to downward diffuse and direct fluxes. Thus, as Fig. 6 illustrates, occurrences of negative PPH random errors (lower two quadrants) are extremely rare. When the PPH overestimates (upper and lower right quadrants), the GWTSA can either overestimate (upper right quadrant) or underestimate (lower right quadrant); in the first case, the GWTSA performs at most times better than PPH (points below the diagonal) since the GWTSA two stream solutions give lower values of albedo (smaller overestimates); in the second case, the GWTSA overcorrects for gridboxes where PPH errors are close to zero, and improves results only as positive PPH errors grow larger.

Shifting our focus now to the distribution of fluxes within the atmosphere, Fig. 7 shows the global daily averaged SW heating rates (HRs) for the four sets of runs (left) as well as the rms errors relative to ICA of the three approximations (right). Both panels clearly demonstrate that the distribution of heating within the atmosphere is captured well by all three approximations on a global basis. This is consistent with the small values of ATMA global mean error shown previously in Fig. 3. Still, an overestimation of heating at the lowest layers of the troposphere by GWTSA can be discerned; this is due to the overestimation of flux transmitted through the cloudy layers above. The opposite happens for PPH and PPH random. GWTSA is performing worse than the PPHs in the higher

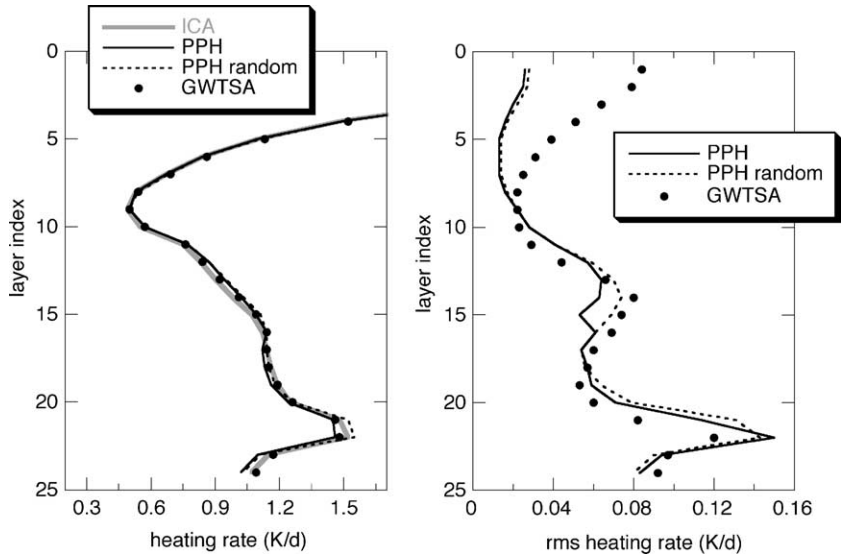

Fig. 7. Daily averaged global SW heating rates (left) and rms errors for the three approximate methods (right).

levels of the atmosphere: Fig. 8 shows that GWTSA actually overestimates the heating consistently at all latitudes (max. value: ~ 0.14 K/day), but the magnitude of the error is still very small when compared to the large absolute values of HR in the upper atmosphere

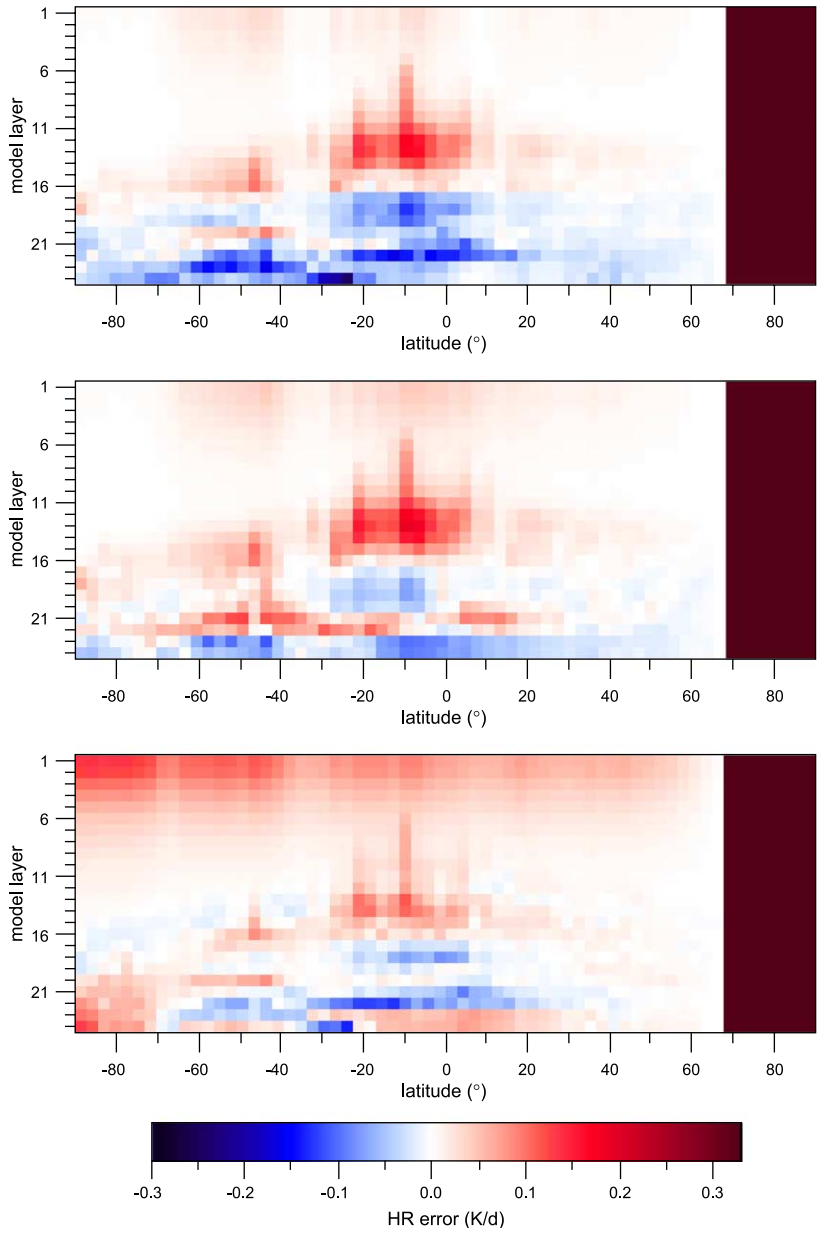

Fig. 8. Daily averaged zonal SW heating rate errors. Top: PPH; middle: PPH random; bottom: GWTSA.

(global HR value of topmost layer: ~ 10.7 K/day). We have not been able to find a conclusive explanation for these overestimates, but one of our hypotheses is that it may be related to the new two-stream PPH solutions for diffuse incidence (which in this case mostly comes from the layers below) implemented in the GWTSA version of the CORAM for clear skies. The remaining features in Fig. 8 show the expected behavior with larger HR errors in the SH than the NH, due to higher insolation, PPH overestimates high in the atmosphere paired with underestimates in the lower atmosphere, and overall improvements (except for the very top layers as previously mentioned) when the GWTSA is introduced. Note that the top panel of Fig. 8 resembles Fig. 8, panel (e) of Räisänen et al. (in press) showing the same quantity for the same input dataset, but from a different CORAM also applying a maximum-random overlap (MRO) approximation.

5. LW experiments

The LW CORAM was only used unmodified with ICA and PPH runs performed using the methodology described above for the SW experiments. Note that in the ICA calculations the subgrid variability of temperatures had a negligible influence on the results (echoing similar results by Fu et al., 2000) and was ignored. The broadband surface emissivities of Räisänen (1999) were used for these runs and surface temperatures were set equal to the average temperature of the lowest CRM layer (CAM surface temperatures were not available). Again, the ozone profile of a midlatitude summer atmosphere was used in all gridboxes.

The figures summarizing the results are similar to those shown previously for the SW case: Fig. 9 shows the globally averaged mean errors and rms errors of PPH for all gridboxes and for overcast (“ovc”) gridboxes only, for the following quantities: outgoing LW radiation (OLR), net flux absorbed at the surface (NSFC), and net flux absorbed within the atmosphere (ATMA). Fig. 10 shows the zonally averaged results for these

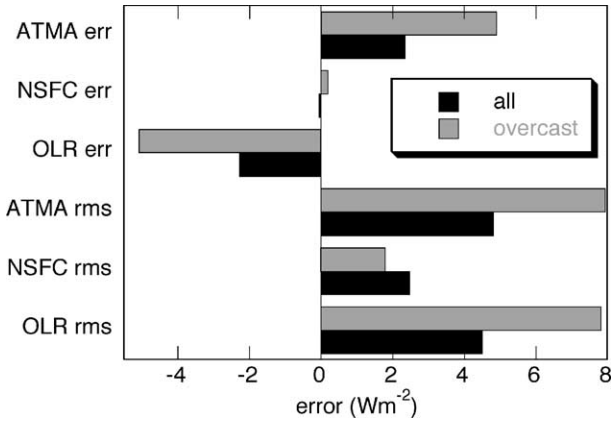

Fig. 9. Daily averaged global LW flux errors of PPH.

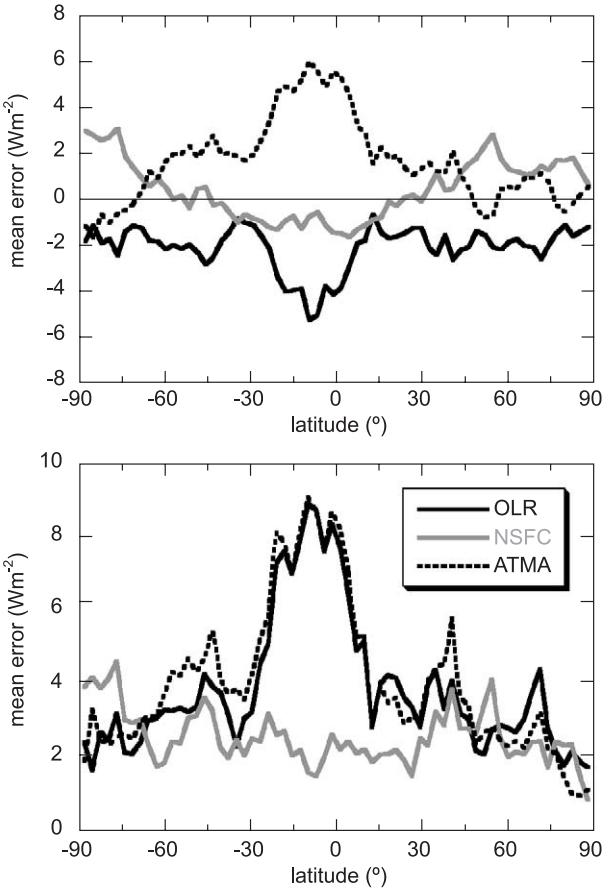

Fig. 10. Daily averaged zonal LW flux mean errors of PPH for OLR, NSFC, ATMA (top), and corresponding rms errors (bottom).

quantities. Fig. 11 shows the globally averaged LW HRs (thus the negative sign) for ICA and PPH (left) and the PPH rms errors (right). Fig. 12 shows zonally averaged HR errors of PPH. Results are again daily averaged over all 24 snapshots, and positive mean error values indicate overestimate relative to the ICA.

It is immediately apparent that the results are consistent with the conventional wisdom that cloud water horizontal inhomogeneity is less important for LW boundary fluxes than in the SW. Global PPH errors for OLR and ATMA are of opposite sign and ~ 2 W m^{-2} in absolute value (underestimates for OLR, as in Fu et al., 2000, albeit quite lower than their cirrus-specific value of ~ -14 W m^{-2}, which is for overcast conditions), and the NSFC error is consequently near zero; notice however that the latter is the result of canceling errors since the rms error exceeds 2 W m^{-2}. Additional evidence of the fortuitous canceling of errors in the global average is provided in Fig. 10, which reveals a strong latitudinal structure in the errors. These results agree almost exactly with

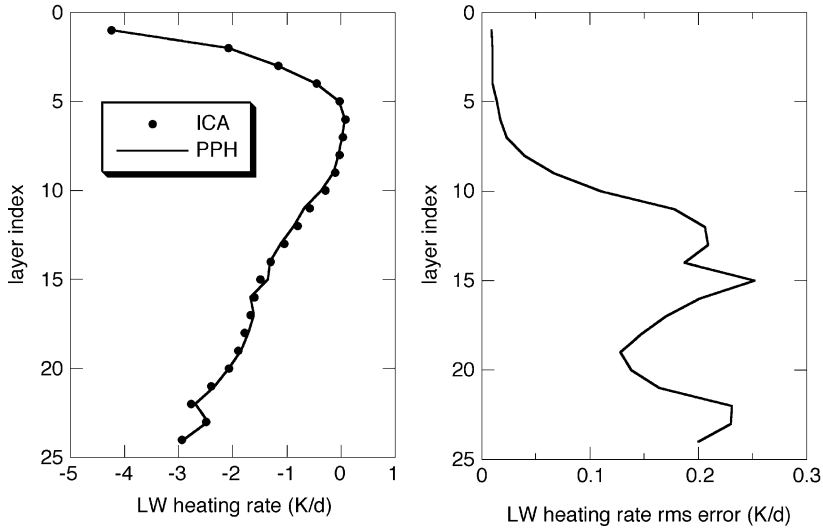

Fig. 11. Daily averaged global LW heating rates (left) and rms errors for PPH (right).

counterpart results in Räisänen et al. (in press, Fig. 7, panels (e) and (h)). In contrast to the SW, but still not unexpectedly, the errors are more symmetric with respect to the equator which is again the area characterized by the largest error magnitudes (Fig. 10). Errors in the HR are very small for global averages (Fig. 11) and have a zonal distribution (Fig. 12) somewhat more difficult to associate with the cloud properties distribution of Fig. 1 than in the SW. The largest heating underestimates (i.e. cooling overestimates) occur around the tops of the deep convective clouds of the ITCZ (consistent with the convex non-linear

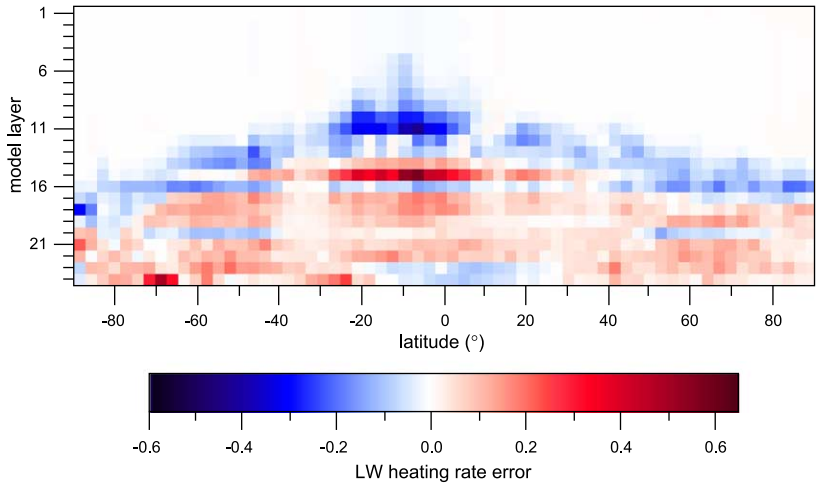

Fig. 12. Daily averaged zonal LW heating rate errors of PPH.

dependence of cloud emissivity on optical depth). For the middle layers of the atmosphere, the net imbalance of PPH fluxes yields overestimates of heating (i.e. underestimates of cooling) in most regions, the combined result of neglecting inhomogeneity for upward and downward cloud emissions. Once again, our results mirror the MRO results by Räisänen et al. (in press, Fig. 8, panel (f)).

6. Conclusions

The results shown in this paper exemplify the generally good performance (compared, for example, to current accuracy of the global TOA energy budget from satellites) of the SW and LW CORAMs by Chou and collaborators, currently implemented in a variety of GSFC GCMs. This good performance pertains to experiments where mean profiles of heterogeneous cloud fields from an atmospheric GCM with a super parameterization (Khairoutdinov et al., in press) are used as input in radiative transfer calculations.

In the SW case, with no subgrid variability information provided, but with perfect profiles of mean water path and cloud fraction as input, the global mean errors, with respect to ICA, of the original PPH-like code are less than 4 W m^{-2} for fluxes at the atmospheric boundaries and 0.3 W m^{-2} for the flux absorbed within the atmosphere. Zonal HR errors are always below 0.3 K/day with overestimates for high clouds and underestimates for low clouds. Zonal flux errors are larger in the Tropics (reaching $\sim$ 10 W m^{-2}) where the thickest and most inhomogeneous clouds are encountered, and larger in the SH than in the NH, mainly because of the greater available solar energy. PPH overestimates reflected flux and underestimates by almost the same amount the flux absorbed at the surface, therefore producing very small errors for the flux absorbed by the atmosphere. When the scaling of optical depth and the overlap assumptions associated with it are removed from the original SW CORAM and the random overlap assumption applied everywhere, the deterioration in performance is notable. On the other hand, implementation of the GWTSA yields substantial improvements in overall performance. Also, GWTSA has significantly lower rms errors than the other two approximations, indicating that cancellation of errors in spatial averages is less extensive.

In the LW case, PPH underestimates OLR and overestimates absorbed flux in the atmosphere by almost equal amounts ($\sim$ 2 W m^{-2} at global scales), and is therefore almost perfect for NSFC (although this in turn is the net result of underestimates in low and overestimates in high latitudes). Again, the largest flux errors for OLR and ATMA occur in the tropics. The HRs tend to be underestimated (cooling rates overestimated) by the PPH at the higher levels of the troposphere and overestimated (cooling rates underestimated) at lower levels with zonal errors always less than 0.6 K/day.

These results suggest that previous studies demonstrating the inadequacy of plane-parallel models may have unfairly focused on worst case scenarios, and that current radiative transfer algorithms of GCMs may be more capable than previously thought in estimating accurate spatial and temporal averages of radiative fluxes, as long as they are provided with realistic cloud profiles. There is some evidence that when the vertical resolution of these algorithms is increased, even better performance can be achieved (Di Giuseppe and Tompkins, 2003; Barker et al., 2003). It would therefore be useful to

conduct a future study to determine whether the encouraging results shown here retain their quality when a larger set of snapshots from such GCM-super parameterization experiments is used. Another good test for the CORAMs, expected to be feasible in the near future, would be to use input cloud profiles from the upcoming CLOUDSAT and CALIPSO missions (Stephens et al., 2002).

Given the consistently better performance of the GWTSA in the SW CORAM, with only a moderate increase in computational time (the almost threefold increase of the current GWTSA version can be improved using the techniques of Barker and Fu, 2000), a strategy for addressing the issues that would allow its operational implementation in a GCM should be seriously contemplated. The most challenging of these issues will probably be prognosing or diagnosing vertical profiles of v.

Finally, one must keep in mind that even if the errors of the particular SW and LW CORAMs are small, the fact that they appear to be systematic (even for GWTSA) implies that they may be potentially important climatically. Their impact can be fully assessed only with extensive GCM simulations.

Acknowledgements

We would like to thank Petri Räisänen for providing the surface albedos and emissivities. This work was supported by NASA grant NAG5-11631 and the U.S. Department of Energy, under grant DE-AI02-00ER62939, as part of the Atmospheric Radiation Measurement Program.

References

Barker, H.W., 1996. A parameterization for computing grid-averaged solar fluxes for inhomogeneous marine boundary layer clouds: Part I. Methodology and homogeneous biases. J. Atmos. Sci. 53, 2289–2303.

Barker, H.W., Fu, Q., 1999. Modelling domain-averaged solar fluxes for an evolving tropical cloud system. Atmos. Ocean. Opt. 12 (3), 211–217.

Barker, H.W., Fu, Q., 2000. Assessment and optimization of the gamma-weighted two-stream approximation. J. Atmos. Sci. 57, 1181–1188.

Barker, H.W., Stephens, G.L., Fu, Q., 1999. The sensitivity of domain-averaged solar fluxes to assumptions about cloud geometry. Q. J. R. Meteorol. Soc. 125, 2127–2152.

Barker, H.W. and 31 coauthors, 2003. Assessing 1D atmospheric solar radiative transfer models: interpretation and handling of unresolved clouds. J. Clim. 16, 2676-2699.

Cahalan, R.F., Ridgway, W., Wiscombe, W.J., Bell, T.L., Snider, J.B., 1994. The albedo of fractal stratocumulus clouds. J. Atmos. Sci. 51, 2434–2455.

Cairns, B., Lacis, A.A., Carlson, B.E., 2000. Absorption within inhomogeneous clouds and its parameterization in general circulation models. J. Atmos. Sci. 57, 700–714.

Chou, M.-D., Suarez, M.J., 1999. A shortwave radiation parameterization for atmospheric studies. NASA Tech. Memo. 15 (104606), 42.

Chou, M.-D., Suarez, M.J., Ho, C.-H., Yan, M.M.-H., Lee, K.-T., 1998. Parameterizations for cloud overlapping and shortwave single-scattering properties for use in general circulation and cloud ensemble models. J. Clim. 11, 202–214.

Chou, M.-D., Suarez, M.J., Liang, X.-Z., Yan, M.M.-H., 2001. A thermal infrared radiation parameterization for atmospheric studies. NASA Tech. Memo. 19 (104606) (55 pp.).

Chou, M.-D., Lee, K.-T., Yang, P., 2002. Parameterization of shortwave cloud optical properties for a mixture of

ice particle habits for use in atmospheric models. J. Geophys. Res. 107 (D21), AAC 22-1–AAC 22-9 (doi:10.1029/2002JD002061).

Di Giuseppe, F., Tompkins, A.M., 2003. Effect of spatial organization on solar radiative transfer in three-dimensional idealized stratocumulus cloud fields. J. Atmos. Sci. 60, 1774–1794.

Fu, Q., Carlin, B., Mace, G., 2000. Cirrus horizontal inhomogeneity and OLR bias. Geophys. Res. Lett. 27, 3341–3344.

Harshvardhan, Randall, D.A., Corsetti, T.G., 1987. A fast radiation parameterization for atmospheric circulation models. J. Geophys. Res. 92, 1009–1016.

Kato, S., 2003. Computation of domain-averaged shortwave irradiance by a one-dimensional algorithm: incorporating correlations between optical thickness and direct incident radiation. J. Atmos. Sci. 60, 182–193.

Khairoutdinov, M.F., Randall, D.A., 2001. A cloud resolving model as a cloud parameterization in the NCAR Community system model: preliminary results. Geophys. Res. Lett. 28, 3617–3620.

Khairoutdinov, M.F., Randall, D.A., 2003. Cloud resolving modeling of the ARM Summer 1997 IOP: model formulation, results, uncertainties and sensitivities. J. Atmos. Sci. 60, 607–625.

Khairoutdinov, M.F., Randall, D.A., DeMott, C., 2004. Simulations of the atmospheric general circulation using a cloud-resolving model and a super-parameterization of physical processes. J. Atmos. Sci. (in press).

Li, J., Barker, H.W., 2002. Accounting for unresolved clouds in a 1D infrared radiative transfer model: Part II. Horizontal variability of cloud water path. J. Atmos. Sci. 59, 3321–3339.

McFarquhar, G.M., 2001. Comments on ''Parametrization of effective sizes of cirrus-cloud particles and its verification against observations'' by Z. Sun, and L. Rikus. Q. J. R. Meteorol. Soc. 127, 261–266.

Meador, W.E., Weaver, W.R., 1980. Two-stream approximations to radiative transfer in planetary atmospheres: a unified description of existing methods and a new improvement. J. Atmos. Sci. 37, 630–643.

Oreopoulos, L., Barker, H.W., 1999. Accounting for subgrid-scale cloud variability in a multi-layer 1D solar radiative transfer algorithm. Q. J. R. Meteorol. Soc. 126, 301–330.

Räisänen, P., 1999. Effect of vertical resolution on cloudy-sky radiation calculations: tests with two schemes. J. Geophys. Res. 104, 27407–27419.

Räisänen, P., Barker, H.W., Khairoutdinov, M.F., Li, J., Randall, D.A., 2004. Stochastic generation of subgrid-scale cloudy columns for large-scale models. Q. J. R. Meteor. Soc. (in press).

Rossow, W.B., Delo, C., Cairns, B., 2002. Implications of the observed mesoscale variations of clouds for the Earth's radiation budget. J. Clim. 15, 557–585.

Stephens, G.L., Vane, D.G., Boain, R.J., Mace, G.G., Sassen, K., Wang, Z., Illingworth, A.J., O'Connor, E.J., Rossow, W.B., Durden, S.L., Miller, S.D., Austin, R.T., Benedetti, A., Mitrescu, C., and the CloudSat Science Team, 2002. The CloudSat mission and the a-train: a new dimension of space-based observations of clouds and precipitation. Bull. Am. Meteorol. Soc. 83, 1771–1790.

Szczap, F., Isaka, H., Saute, M., Guillemet, B., Ioltukhovski, A., 2000a. Effective radiative properties of bounded cascade nonabsorbing clouds: definition of the equivalent homogeneous cloud approximation. J. Geophys. Res. 105, 20617–20633.

Szczap, F., Isaka, H., Saute, M., Guillemet, B., Ioltukhovski, A., 2000b. Effective radiative properties of bounded cascade nonabsorbing clouds: definition of an effective single-scattering albedo. J. Geophys. Res. 105, 20635–20648.

Szczodrak, M., Austin, P.H., Krummel, P.B., 2001. Variability of optical depth and effective radius in marine stratocumulus clouds. J. Atmos. Sci. 58, 2912–2926.

Tian, L., Curry, J.A., 1989. Cloud overlap statistics. J. Geophys. Res. 94, 9925–9935.